

Hard photon flow and photon-photon correlation in intermediate energy heavy-ion collisions

Y. G. Ma*,¹ G. H. Liu,¹ X. Z. Cai,¹ D. Q. Fang,¹ W. Guo,¹ W. Q. Shen,¹ W. D. Tian,¹ and H. W. Wang¹

¹*Shanghai Institute of Applied Physics, Chinese Academy of Sciences, Shanghai 201800, China*

(Dated: January 1, 2018)

Hard photons emitted from energetic heavy ion collisions are very interesting since they do not experience nuclear interaction, and therefore they are useful to explore properties of nuclear matter. We investigated hard photon production and its properties in intermediate energy heavy-ion collisions with the help of the Blotzmann-Uehling-Ulenbeck model. Two components of hard photons are discussed: direct and thermal. The positive directed flow parameter and negative elliptic flow parameter of direct photons are demonstrated and they are anti-correlated to the flows of free protons. The dependencies of hard photon production and anisotropic parameters on impact parameter, beam energy, nuclear equation of state and symmetry energy are also discussed. Furthermore, we investigated the two-photon momentum correlation function from which the space-time structure information of the photon source could be extracted as well as the two-photon azimuthal correlation which could provide another good method to determine the elliptic flow parameter v_2 of direct hard photons.

PACS numbers: 25.75.Ld, 24.10.-i, 21.60.Ka

I. INTRODUCTION

One of the main goals of intermediate energy heavy ion collision (HIC) is to study properties of nuclear matter, especially to determine the nuclear Equation-of-State (EOS). HIC provides a unique means to compress nuclear matter to hot and dense phase within a laboratory environment. The pressures that result from the high densities achieved during such collisions strongly influence on the motion of ejected matter and provide the sensitivity to the EOS. In comparison with the conventional hadronic probes, photons interacting only weakly through the electromagnetic force with the nuclear medium are not subjected to distortions by the final state (neither Coulomb nor strong) interactions and therefore photon delivers an undistorted picture of the emitting source [1–4].

Since the last two decades, many model calculations and experimental facts [1–9] have indicated that in intermediate energy heavy-ion collisions hard photons defined as photons with energies above the giant dipole resonance domain, above 30 MeV in this paper, mainly originate from incoherent proton-neutron bremsstrahlung collisions, namely $p+n \rightarrow p+n+\gamma$. A nice review paper on hard photon was available [3]. These hard photons are emitted from two distinct sources. The first and dominant component denoted as direct hard photon (called as "direct photon" for short) is associated with the first-chance proton-neutron collisions in the initial phase of the heavy-ion reaction. The second one originates from the secondary proton-neutron collisions in the later stage of the reactions when the di-nuclear system tends to be thermalized, accordingly called as thermal hard photon

(called as "thermal photon" for short). Because of their distinct emission sources, direct photons and thermal photons can deliver thermodynamic and dynamical information of hot and dense nuclear matter formed during the various stages of the heavy-ion collisions.

In relativistic heavy ion collisions, photons are also of very interesting since they can be served as one of the potential signals of quark-gluon plasma (QGP) formation, eg., see Ref. [10–13]. A hot QGP radiates a large amount of thermal photons, which dominate the spectra at small transverse momenta, whereas hard processes in nucleon-nucleon scatterings produce large momenta photons. Therefore photon enhancement at low transverse momenta could be seen as a QGP signal, which has been observed at the BNL-Relativistic Heavy-Ion Collider [10]. Similar to the feature of photon production in intermediate energy HIC, photons emitted from the interior of the hot matter no longer interact with the hadronic medium, in contrast to hadronic observables.

The paper is organized as follows. In Sec. II, the simulation tool which we used is briefly introduced and the calculation method of photon production is outlined. Sec. III describes the classification of hard photons and definition of anisotropic flow, and presents the results of the azimuthal asymmetry for direct photons and free protons. In Sec. IV, we discuss the different variables (impact parameter, beam energy and EOS) dependences of the hard photon production and/or anisotropic flow parameters. Sec. V gives the results and discussions on two-photon correlation functions, namely momentum correlation function, which is also called Hanbury-Brown and Twiss (HBT) correlation function, as well as azimuthal correlation function. Finally the summary is given in Sec. VI.

*ygma@sinap.ac.cn

II. BRIEF INTRODUCTION TO THE MODEL AND PHOTON PRODUCTION

A. The Boltzmann-Uehling-Ulenbeck Equation

The transport model is very useful for treating heavy-ion collision dynamics and obtaining important information of nuclear matter. In intermediate energy heavy-ion collisions, the Boltzmann-Uehling-Ulenbeck (BUU) model is an extensively useful tool [14]. The BUU equation takes both Pauli blocking and the mean field into consideration, reads

$$\begin{aligned} \frac{\partial f}{\partial t} + v \cdot \nabla_r f - \nabla_r U \cdot \nabla_p f &= \frac{4}{(2\pi)^3} \int d^3 p_2 d^3 p_3 d\Omega \\ \frac{d\sigma_{NN}}{d\Omega} V_{12} \times [f_3 f_4 (1-f)(1-f_2) - f f_2 (1-f_3)(1-f_4)] \\ \delta^3(p + p_2 - p_3 - p_4). \end{aligned} \quad (1)$$

It is solved with the method of Bertsch and Das Gupta [15]. In Eq. (1), $\frac{d\sigma_{NN}}{d\Omega}$ and V_{12} are in-medium nucleon-nucleon cross section and relative velocity for the colliding nucleons, respectively, and U is the mean field potential including the isospin-dependent term:

$$U(\rho, \tau_z) = a\left(\frac{\rho}{\rho_0}\right) + b\left(\frac{\rho}{\rho_0}\right)^\sigma + C_{sym} \frac{(\rho_n - \rho_p)}{\rho_0} \tau_z, \quad (2)$$

where ρ_0 is the normal nuclear matter density; ρ , ρ_n , and ρ_p are the nucleon, neutron and proton densities, respectively; τ_z equals 1 or -1 for neutrons and protons, respectively; The coefficients a , b and σ are parameters for nuclear equation of state. Three sets of mean field parameters are used, namely the soft EOS with the compressibility K of 200 MeV ($a = -356$ MeV, $b = 303$ MeV, $\sigma = 7/6$), and the semi-soft EOS with K of 235 MeV ($a = -218$ MeV, $b = 164$ MeV, $\sigma = 4/3$), and the hard EOS with K of 380 MeV ($a = -124$ MeV, $b = 70.5$ MeV, $\sigma = 2$). C_{sym} is the symmetry energy strength due to the density difference of neutrons and protons in nuclear medium, which is important for asymmetry nuclear matter (here $C_{sym} = 32$ MeV is used), but it is trivial for the symmetric system studied in the present work.

B. Production cross sections of bremsstrahlung hard photon

The BUU model was shown to be very successful in describing the bulk properties of the reaction and nucleon emission in intermediate-energy heavy-ion collisions. In addition, the proton-neutron bremsstrahlung photon can be simulated as well in the model. For determining the elementary double-differential hard photon production cross sections on the basis of individual proton-neutron bremsstrahlung, the hard-sphere collision was adopted from Ref. [16], and modified as in Ref. [17] to allow for

energy conservation. The double differential probability is given by

$$\frac{d^2 \sigma^{elem}}{dE_\gamma d\Omega_\gamma} = \alpha_c \frac{R^2}{12\pi} \frac{1}{E_\gamma} (2\beta_f^2 + 3\sin^2 \theta_\gamma \beta_i^2). \quad (3)$$

Here R is the radius of the sphere, α_c is the fine structure constant, β_i and β_f are the initial and final velocity of the proton in the proton-neutron center of mass system, and θ_γ is the angle between incident proton direction and photon emitting direction. More details for the model can be found in Ref. [14, 18].

III. AZIMUTHAL ASYMMETRY OF HARD PHOTONS

A. Definitions of direct photons and thermal photons

In the present work, we simulate the reaction of $^{40}\text{Ca} + ^{40}\text{Ca}$ collisions in most cases. Sometimes $^{48}\text{Ca} + ^{48}\text{Ca}$ and $\text{Kr} + \text{Ni}$ are also simulated.

Fig. 1(a) and (b) show the time evolutions of the production rate of bremsstrahlung hard photons and of system densities, including both maximum density (closed circles) and average density (open circles), respectively, for $^{40}\text{Ca} + ^{40}\text{Ca}$ collisions at 60A MeV in the centrality of 40%–60%. It is found that the hard-photon production rate is sensitive to the density oscillations during the whole reaction evolution. With the increase in density when the collision system is in the compression stage, the system produces more hard photons. In contrast, when the system starts to expand, the hard photon production rate decreases. Actually, the density oscillation of the colliding heavy-ion systems can be observed in the experiments via hard-photon interferometry measurements [1, 6, 19] as well as dynamical dipole γ radiation [20–22]. Apparently, hard photons are mostly produced at the early stage of the reaction. Thereafter we call these photons, emitted before the time of the first maximum expansion of the system ($t \sim 65$ fm/c in $\text{Ca} + \text{Ca}$ at 60A MeV), as direct hard photons (on the left side of the blue dashed line in Fig. 1(a)). It is also coincident with the definition in the Sec.I of direct hard photons. We call the residual hard photons producing in the later stage as thermal hard photons (on the right side of blue dashed line in Fig. 1). In this way, we can identify the producing photon as either direct or thermal by the emission time of photons in the present simulation. We notice that the production rate of thermal photon tends to decrease for later time, after 300 fm/c for $\text{Ca} + \text{Ca}$ at 60A MeV, which can be understood by the decrease of n-p collisions in an expanding system. However, the hard photon yields in the later stage after 300 fm/c is relative small fraction of the total thermal hard photon emission. Also, in the following calculations, we mainly focus on direct hard photons which dominate the yield and do not depend on the time evolution for the later stage.

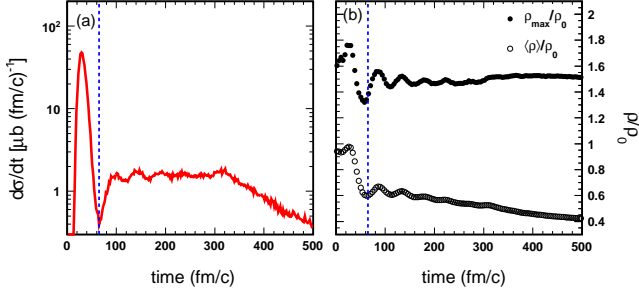


FIG. 1: (Color online) (a) Time evolution of hard photon production rate for the reaction $^{40}\text{Ca} + ^{40}\text{Ca}$ at 60A MeV in 40%–60% centrality. The EOS parameters with the compressibility K of 235 MeV are used; (b) Time evolution of reduced maximum density ρ_{max}/ρ_0 (closed circles) and reduced average density $\langle\rho\rangle/\rho_0$ (open circles) of the whole reaction system in the same reaction. The blue dashed line represents the time when till the first expansion stage, and in the panel (a) it separates direct hard photons (on the left side) and thermal hard photons (on the right side).

For an example, Fig. 2 demonstrates that the direct and thermal hard photons for 60A MeV $^{40}\text{Ca} + ^{40}\text{Ca}$ collisions with a compressibility K of 235 exhibit different spectral shapes: thermal photons give rise to a softer energy spectral than direct ones. In the nucleon-nucleon center-of-mass system, the photon spectrum can be described by the function:

$$\frac{d\sigma}{dE_\gamma} = I_0 e^{-\frac{E_\gamma}{E_0}}, \quad (4)$$

where I_0 is a normalization constant and E_0 is the slope parameter, which reflects the apparent source temperature of the photon emission source. The slope parameter E_0 depends on the bombarding energy and on the average intrinsic momentum of the participant nucleons. As less energy is available on average in second-chance n - p collisions than in first-chance collisions because most of the projectile kinetic energy is damped, the thermal-photon spectrum becomes much softer. If one adds the two sources together in the photon spectrum, one obtains an empirical photon spectrum of the form [1, 8, 9]:

$$\frac{d\sigma}{dE_\gamma} = K_d e^{-\frac{E_\gamma}{E_0^d}} + K_{th} e^{-\frac{E_\gamma}{E_0^{th}}}, \quad (5)$$

with the constant $K_{d,th}$ defined by:

$$I_{d,th} = K_{d,th} \int_{E_{30}}^{\infty} e^{-\frac{E_\gamma}{E_0^{d,th}}} dE_\gamma = K_{d,th} E_0^{d,th} e^{-\frac{E_{30}}{E_0^{d,th}}}. \quad (6)$$

$I_{d,th}$ represents the intensity of each photon source, d stands for the direct photon and th for stands for the thermal photon. However, we notice that the change in slope of the photon yield could be also affected by the $1/E_\gamma$ factor which enters the elementary $np - np\gamma$ bremsstrahlung probability [23]. In this case, Eq. 5

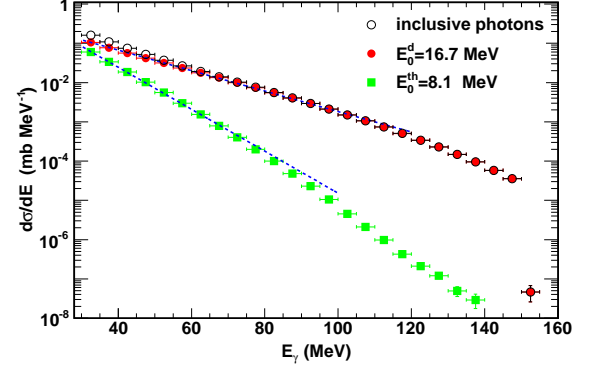


FIG. 2: (Color online) Kinetic energy spectrum of direct photons and thermal photons for inclusive events of $^{40}\text{Ca} + ^{40}\text{Ca}$ at 60A MeV with the compressibility K of 235 MeV. Black dots and blue dots represent the direct photons and thermal photons, respectively. Lines represent the exponential fits with th Eq. 5.

should be changed into

$$\frac{d\sigma}{dE_\gamma} = \frac{(K_d)'}{E_\gamma} e^{-\frac{E_\gamma}{(E_0^d)'}} + \frac{(K_{th})'}{E_\gamma} e^{-\frac{E_\gamma}{(E_0^{th})'}}. \quad (7)$$

In the next paragraph, we will compare the difference for the fitted slope with Eq. 5 and Eq. 7.

As shown in the inset of the figure, the slope parameters of direct photons and thermal photons are 16.7 and 8.1 MeV, respectively, for inclusive events of $^{40}\text{Ca} + ^{40}\text{Ca}$ collisions at 60A MeV with an incompressibility K of 235 MeV if we fit the spectrum with the Eq. 5. However, Eq. 7 will give a larger slope value, namely 22.5 and 9.8 MeV, respectively, which is 35% and 20% higher than the fits without the $1/E_\gamma$ factor (not plotted in the figure). With two different fit formulas, we put the impact parameter dependence of the slope parameter together in Fig. 3. A remarkable difference is seen between the slope values with and without the $1/E_\gamma$ factor, i.e. Eq. 7 gives a higher apparent photon temperature than Eq. 5. In some previous experimental analysis [1, 8, 9], Eq. 5 was mostly used to extract the apparent slope, but this is probably not correct since a factor $1/E_\gamma$ in front of the exponential form can be derived from their elementary cross section [see Eq. 3]. On the other hand, the slope of hard photons displays a slight decreasing behavior with increasing impact parameter, indicating that the emission source becomes cooler in peripheral collisions. Moreover, direct photons are hotter than thermal photons as we expected.

B. Definition of anisotropic flows

It is well known that collective flow is an important observable in heavy ion collisions and it can carry some essential information on the nuclear matter, such as the nuclear equation of state [24–34]. Anisotropic flows are

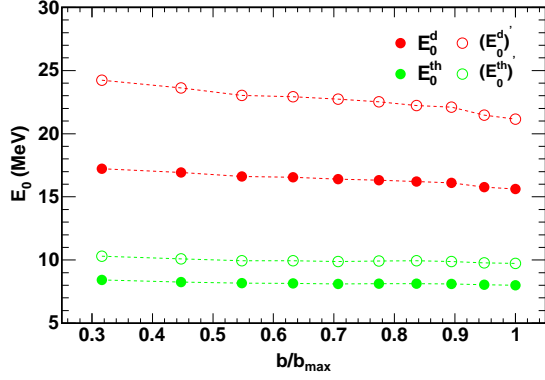


FIG. 3: (Color online) The slope parameters of direct and thermal hard photons as a function of impact parameter for $^{40}\text{Ca}+^{40}\text{Ca}$ at 60A MeV with the incompressibility K of 235 MeV. Open symbols represent the results from the Eq. 7 and solid symbols are from Eq. 5.

defined as different n th harmonic coefficients v_n of an azimuthal Fourier expansion of the particle invariant distribution [25]

$$\frac{dN}{d\phi} \propto 1 + 2 \sum_{n=1}^{\infty} v_n \cos(n\phi), \quad (8)$$

where ϕ is the azimuthal angle between the transverse momentum of the particle and the reaction plane. Note that in the coordinate system the z -axis is along the beam axis, and the impact parameter axis is labeled as the x -axis.

The first harmonic coefficient v_1 represents the directed flow,

$$v_1 = \langle \cos\phi \rangle = \left\langle \frac{p_x}{p_t} \right\rangle, \quad (9)$$

where $p_t = \sqrt{p_x^2 + p_y^2}$ is the transverse momentum. The second harmonic coefficient v_2 represents the elliptic flow which characterizes the eccentricity of the particle distribution in momentum space,

$$v_2 = \langle \cos(2\phi) \rangle = \left\langle \frac{p_x^2 - p_y^2}{p_t^2} \right\rangle. \quad (10)$$

C. Directed and elliptic flows of direct photons and free protons

In relativistic heavy-ion collisions directed and elliptic flows of hard photons have been recently reported in the experiments and through theoretical calculations [35–39], demonstrating a very useful tool for exploring the properties of hot dense matter. However, there are no experimental data available so far on the flow of hard photons in intermediate energy heavy ion collisions. In

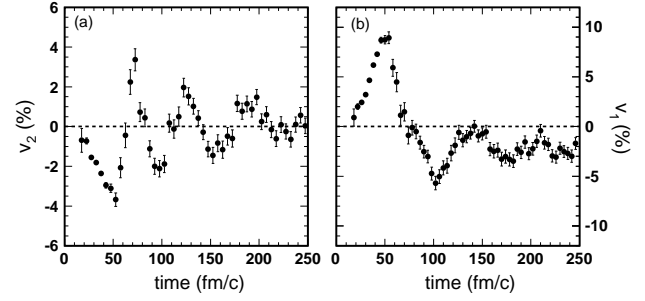


FIG. 4: The time evolution of elliptic flow (v_2) of hard photons (a) and directed flow (v_1) (b) for 60A MeV Ca + Ca collisions at centrality of 40-60%.

this context, here we calculate directed transverse or elliptic flows in intermediate energy heavy ion collisions. In addition, given that hard photons mostly originate from bremsstrahlung by individual proton-neutron collision and that free nucleons are also emitted from nucleon-nucleon collisions, therefore it will be interesting to compare flows of protons and photons.

Fig. 4 shows the time evolution of the average values of directed flow and elliptic flow of the photons. Considering the nearly symmetric behavior for directed flow versus rapidity, here we calculate the average v_1 over only the positive rapidity range, which can be taken as a measure of the directed flow.

From Fig. 4, the directed flow of photons show rapid rising with positive values during the compression stage and later on it decreases to even negative value. Afterwards, the directed flow remains negative since the system is never compressed. For elliptic flow, the behavior shows contrary trend to the v_1 and later on it shows oscillation for thermal photon emission. The times corresponding to the peak or valley values of flows roughly keep synchronized with the compression or expansion oscillation on the system evolution as shown in Fig. 1(b).

From the above calculations, we learn that direct photons are preferentially emitted in the out-of-plane (negative v_2) direction and thermal photons are emitted from a thermalizing system which makes their emission more isotropic (i.e. the oscillated elliptic flow) than the direct ones produced in the pre-equilibrium stage. In addition, thermal photons contribute less than 30% of the total yield of hard photon in the present model. Therefore we will focus on direct hard photons to discuss the flow results.

The quantity of directed transverse flow at mid-rapidity can be also defined by the slope: $F = \left. \frac{d\langle p_x \rangle}{d(y)_{c.m.}} \right|_{(y)_{c.m.}=0}$, where $(y)_{c.m.}$ is the rapidity of particles in the center of mass and $\langle p_x \rangle$ is the mean in-plane transverse momentum of photons or protons in a given rapidity region. In Fig. 5(a) and (b), we show $\langle p_x \rangle$ plotted versus the $c.m.$ rapidity $y_{c.m.}$ for direct hard photons (a) as well as $\langle p_x \rangle$ plotted versus the reduced $c.m.$ rapid-

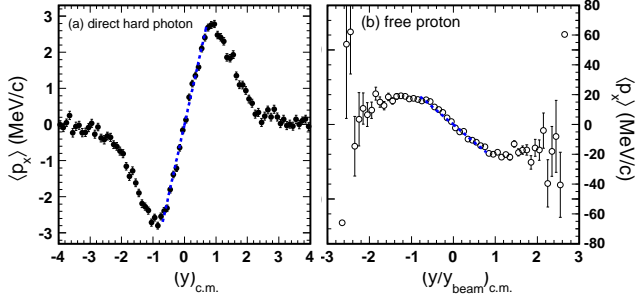


FIG. 5: (Color online) (a) Average in-plane transverse momentum of direct hard photons as a function of $c.m.$ rapidity for 60A MeV Ca + Ca collisions in the semi-central centrality of 40 – 60%. The dashed line segment is a fit over the mid-rapidity region $-0.5 \leq y_{c.m.} \leq 0.5$. (b) Same as the left panel but for free protons. The dashed line segment is a fit over the mid-rapidity region $-0.5 \leq (y/y_{beam})_{c.m.} \leq 0.5$.

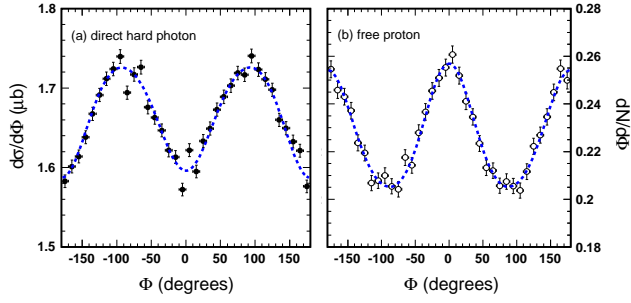


FIG. 6: (Color online) (a) and (b) is the azimuthal distribution of direct photons and of free protons, respectively, for 60A MeV Ca + Ca collisions in the semi-central centrality of 40 – 60%. Both of them are fitted to the 4-th order Fourier expansion.

ity $(y/y_{beam})_{c.m.}$ for free protons (b) for 60A MeV Ca + Ca collisions in the semi-central centrality of 40 – 60%. The EOS parameters with the compressibility K of 235 MeV are used. The errors shown are only statistical. For emitted proton (free proton), we identify it in the BUU calculation as its local density $\rho < 1/8\rho_0$. We take the values of flows when the system has been already in the freeze-out time at 180 fm/c. A good linearity is seen in the mid-rapidity region $(-0.5, 0.5)$ and the slope of a linear fit can be defined as the magnitude of directed transverse flow. The extracted value for the directed transverse flow of direct hard photons is about +3.9 MeV/c, and that of free protons is about -23.7 MeV/c. Thus direct hard photons do exist the directed transverse flow even though the absolute value is smaller than the proton's flow, and the sign of its flow is just opposite to that of free protons.

In order to extract the value of elliptic flow and reduce the error of fits, we fit the azimuthal distribution to the 4th order Fourier expansion. Fig.6 shows an example for such fits with the elliptic flow parameter $v_2 = -2\%$ for photons and $v_2 = 5.5\%$ for protons.

Fig. 7 shows the differential elliptic flow of direct hard

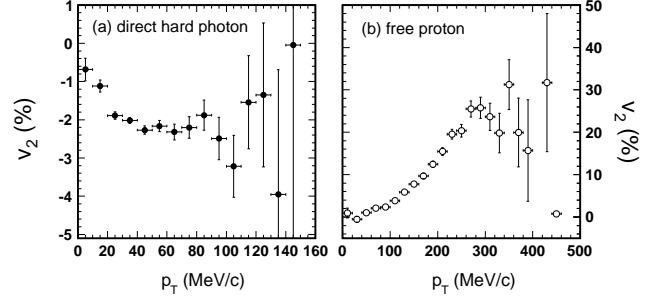


FIG. 7: Elliptic flows (v_2) for direct hard photons (a) and free protons (b) as a function of transverse momentum (p_T) for 60A MeV Ca + Ca collisions in the semi-central centrality of 40 – 60%.

photons (a) and of free protons (b) as a function of transverse momentum p_T for $^{40}\text{Ca} + ^{40}\text{Ca}$ at 60A MeV. Similar to the directed transverse flow, the values of elliptic flow of direct hard photons and of free protons also have an opposite signs at this reaction energy, i.e., reflecting a different preferential transverse emission in the direction of out-of-plane or in-plane, respectively. Meanwhile, absolute flow values for photons are smaller than the proton's like the behavior of transverse flow. Except of the opposite sign, we see that both elliptic flows have similar tendency with the increasing of p_T , i.e., their absolute values increase at lower p_T , and becomes gradually saturated, especially for direct hard photons.

To explain the correlation of the collective flow between direct hard photons and free protons indicating above, we should note that flows of direct hard photons originate from the individual proton-neutron collisions. As Eq. 3 shows, we can roughly consider that in the individual proton-neutron center of mass system, in directions perpendicular to incident proton velocity, i.e. $\theta_\gamma = 90^\circ$, the possibility of hard photon production is much larger than the parallel direction, actually it is also in agreement with the theoretical calculations and the experiments [40, 41]. As a whole, the flow of hard photons should be correlated with the collective movement of the nucleons, and presents an opposite behavior. Consequently, flows of hard photons and of free nucleons exhibit an opposite character.

IV. DEPENDENCES OF HARD PHOTON PRODUCTION AND FLOW ON SOME VARIABLES

A. Impact parameter dependence

It is well known that anisotropic flow mainly originates from the initial asymmetric overlap zone of colliding nuclei which induces different pressures or rotational collective motion of the participant region and leads to anisotropic emission of the particles. Peripheral collisions have more initial asymmetry in overlap zone than central

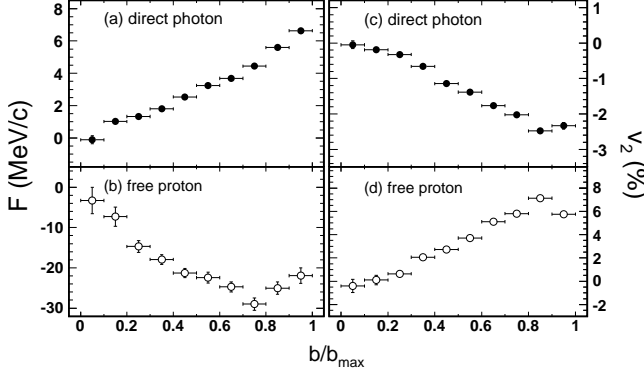


FIG. 8: (a) and (b) are the directed transverse flow parameter F of direct photons and free protons, respectively, as a function of the reduced impact parameter for the reaction $^{40}\text{Ca} + ^{40}\text{Ca}$ collisions at 60A MeV. (c) and (d) same as above but for elliptic asymmetry coefficient v_2 .

collisions, thus more anisotropic emission of the particles is expected. Therefore anisotropic emission shall be sensitive to impact parameter.

Here we simulate the reaction $^{40}\text{Ca} + ^{40}\text{Ca}$ collisions at 60A MeV, and use the EOS parameters with the compressibility K of 235 MeV for the nuclear mean field U . Fig. 8 (a) and (b) shows the directed transverse flow parameter F of direct photons and free protons, respectively, as a function of the reduced impact parameter (i.e. normalized by the maximum impact parameter). Fig. 8 (c) and (d) are the same as (a) and (b) but for elliptic asymmetry coefficient v_2 . We can see that both F and v_2 of direct photons and free protons have the similar tendency with impact parameter, i.e. their absolute values increase with the impact parameter except of slightly decreasing in very peripheral collisions for v_2 . We also see that at all impact parameters, in contrast to the negative directed transverse flow and positive elliptic flow of free protons, direct photons show the positive F and the negative v_2 , i.e. the anisotropy is shifted by a phase $\pi/2$. It agrees with the previous conclusion that the azimuthal asymmetry of direct photons is anti-correlated with the corresponding free proton's flow.

B. Beam energy dependence

In Fig. 9 we show the directed transverse flow parameter F and elliptic asymmetry coefficient v_2 of direct photons and free protons, respectively, as a function of beam energy for the Ca + Ca reaction at (40 – 60%) centrality. In the beam energy range studied here, same as the impact parameter dependence, the opposite signs of F and v_2 between direct photons and free protons are also anticorrelated. Moreover, except for the opposite sign, directed transverse flow parameter F of direct photons and free protons have similar structures with the increas-

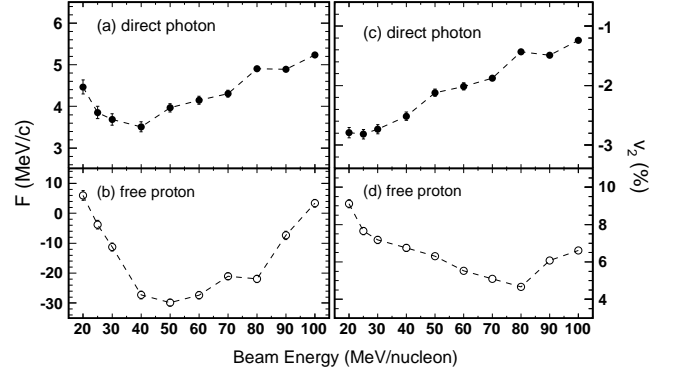


FIG. 9: (a) and (b) is the directed transverse flow parameter F of direct photons and free protons, respectively, as a function of beam energy for the reaction which is the same as Fig. 8 but only semi-central events (40 – 60%). (c) and (d) same as above but for elliptic asymmetry coefficient v_2 .

ing of beam energy. The value of direct photon elliptic asymmetry coefficient v_2 increases with beam energy from negative to positive, a tendency similar to available experimental results on hard photons in relativistic heavy-ion collisions.

C. EOS and symmetry energy dependences

In this section we will discuss the nuclear equation of state and its symmetry energy term dependences of hard photon production. In our calculations, the single-particle potential taken as the Skyrme parameterized mean field potential including symmetry potential is shown below

$$U^{n(p)}(\rho) = \alpha\left(\frac{\rho}{\rho_0}\right) + \beta\left(\frac{\rho}{\rho_0}\right)^\sigma + V_{asy}^{n(p)}(\rho, \delta), \quad (11)$$

where the coefficients a , b and σ are parameters for nuclear equation of state which is determined by the nuclear saturation property and the incompressibility K of symmetric nuclear matter; δ is the isospin-asymmetry parameter, $\delta = (\rho_n - \rho_p)/(\rho_n + \rho_p)$, and $V_{asy}^{n(p)}(\rho, \delta)$ is the symmetry potential of neutrons (protons).

First, we only investigate the effects of the incompressibility K on the hard photon production in symmetric reaction system. In the Skyrme potential, we take the incompressibility K as 200 MeV, 235 MeV and 380 MeV, in which the first two correspond to soft and semi-soft potential and the last one corresponds to hard potential as we introduced in Sec.II A.

Because of the sensitivity to the density oscillations of colliding system, hard photon should be also dependent of the EOS of nuclear matter, especially for thermal hard photons [6, 7]. Actually as shown in Fig. 10, photon production shows its sensitivity to the compressibility, especially for thermal photon which are produced after $t \sim 80$

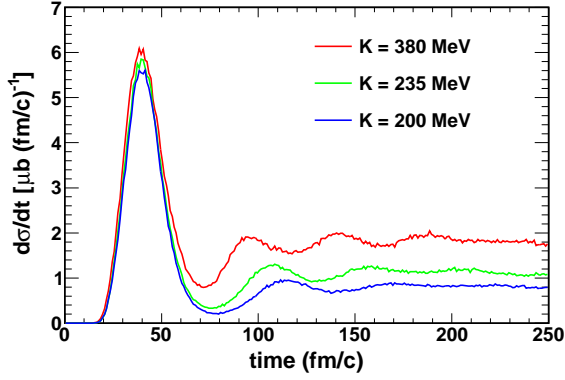


FIG. 10: (Color online) Time evolution of production rate of bremsstrahlung photons with time for inclusive events of $^{40}\text{Ca} + ^{40}\text{Ca}$ at 30A MeV. Different EOS are used, namely the hard EOS, the semi-soft EOS and the soft EOS, respectively.

fm/c. It shows that the stiffer the EOS, the higher multiplicity the thermal photons. In contrast, direct photons are produced by the first channel neutron-proton bremsstrahlung, their production rate only weakly depends on EOS since direct hard photons are emitted by the first channel n-p scattering when the system is in a highly nonequilibrium state during the compression stage, and they do not have enough times to feel the EOS.

Shown in Fig. 11 is the time evolution of inclusive hard photon multiplicity from the symmetric reaction system $^{40}\text{Ca} + ^{40}\text{Ca}$ at 60A MeV. We can see that at this energy, for different incompressibility K , multiplicities of hard photons produced in the early stage of collisions are nearly equivalent and later they show a clear correlation with incompressibility K . Corresponding to direct and thermal photons, this indicates that direct photon production is not sensitive to incompressibility K , because at this reaction energy, comparable with two-body interactions, mean field can be neglected in producing hard photons in the early stage of collisions. However, there is a correlation between K and thermal photon production, with larger K producing more thermal photons.

For the magnitude of flow parameters F and v_2 , comparisons are made for different equation of state. Fig. 12 shows the F and v_2 as a function of impact parameter with different EOS. Generally, the directed flow becomes larger with the increasing of stiffness of the EOS, whereas the elliptic flow becomes smaller.

In order to study the effects of symmetry potential, we now set incompressibility K as 380 MeV. We mainly consider three kinds of symmetry potential: (1) the symmetry potential is neglected, that is

$$V_{asy}^{(0)}(\rho, \delta) = 0; \quad (12)$$

(2) the symmetry potential is a linear function of isospin-

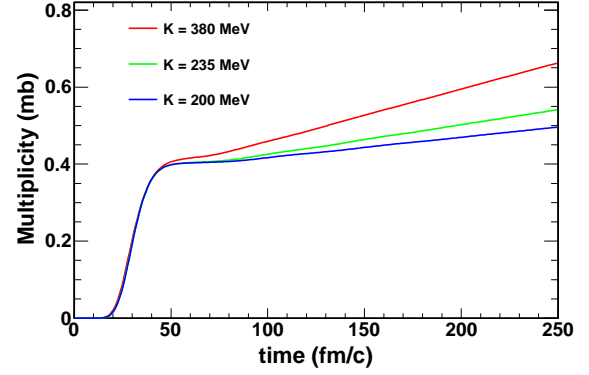


FIG. 11: (Color online) Time evolution of hard photon multiplicity with different incompressibility K for the reaction $^{40}\text{Ca} + ^{40}\text{Ca}$ at 60A MeV.

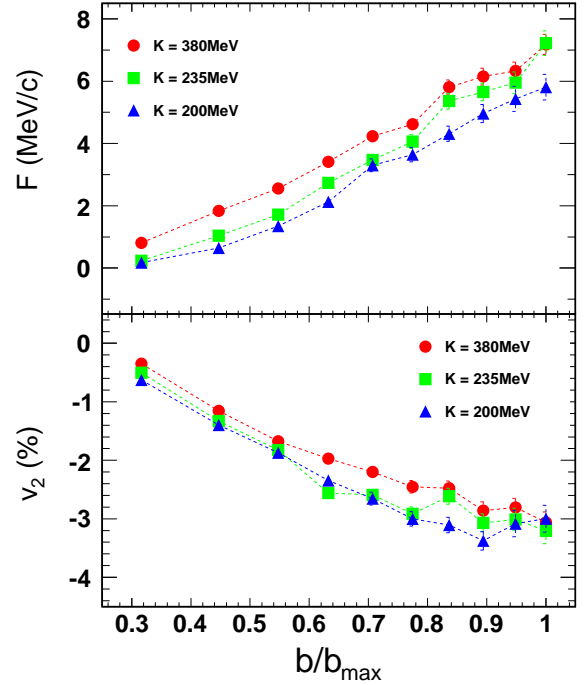


FIG. 12: (Color online) Directed flow parameter (F) and elliptic flow (v_2) as a function of impact parameter with different EOS parameters for Ca + Ca at 30A MeV.

asymmetry parameter δ , that is

$$V_{asy}^{(1)}(\rho, \delta) = C_{sym} \delta \tau^{n(p)}, \quad (13)$$

where $C_{sym} = 32$ MeV, $\tau^n = 1$, $\tau^p = -1$;

(3) the Li et al. single-particle potential from the parametrization of nuclear symmetry energy used in Ref. [42] for studying the properties of neutron stars, that is $E_{sym}(\rho) = E_0(\rho_0)(\frac{\rho}{\rho_0})^\gamma$, Li *et al.* derived a single-

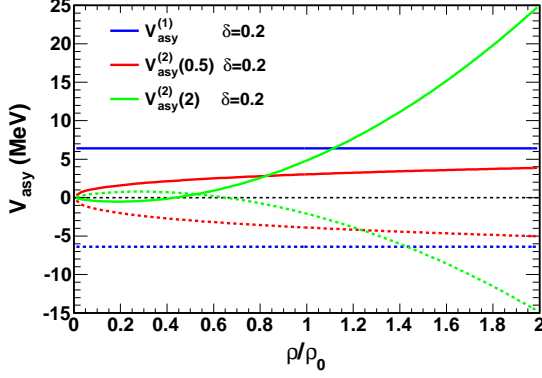


FIG. 13: (Color online) Different symmetry potential which is used in the present model calculation as a function of density for an isospin asymmetry of $\delta = 0.2$ and the γ parameters of 0.5 (red line) and 2.0 (green line), respectively. Solid lines are for neutrons and dashed lines for protons.

particle symmetry potential as [43]:

$$V_{asy}^{(2)}(\rho, \delta) = \left[E_0(\rho_0)(\gamma - 1)\left(\frac{\rho}{\rho_0}\right)^\gamma + 4.2\left(\frac{\rho}{\rho_0}\right)^{2/3} \right] \times \delta^2 + \left(E_0(\rho_0)\left(\frac{\rho}{\rho_0}\right)^\gamma - 12.7\left(\frac{\rho}{\rho_0}\right)^{2/3} \right) \delta \tau^{n(p)}, \quad (14)$$

where $\tau^n=1$, $\tau^p=-1$, $E_0(\rho_0)$ sets as 30 MeV in this paper, and parameter γ represents the stiffness of the symmetry energy. In the following, we consider two cases of $\gamma = 0.5$ and 2, respectively, corresponding to soft and stiff symmetry energy, to explore the effects of different symmetry potential.

The symmetry potentials for neutron and proton with $\delta = 0.20$ is plotted in Fig. 13, where the red line represents $V_{asy}^{(1)}$, and the blue and green lines represent $V_{asy}^{(2)}$ for γ parameters of 0.5 and 2.0 for neutrons (upper branch) and protons (lower branch), respectively. For small isospin asymmetry and density near ρ_0 the above symmetry potentials reduce to the well known Lane potential which varies linearly with δ [44]. Generally, the repulsive/attractive symmetry potential for neutrons/ protons increases with density.

Fig. 14 shows the time evolution of inclusive hard photon multiplicity in the reaction $^{48}\text{Ca} + ^{48}\text{Ca}$ at 60A MeV. In order to separate the effects of symmetry potential from the incompressibility, we set K as a constant 380 MeV. Fig. 14 presents the effects of different symmetry potentials on hard photon productions. Same as the incompressibility K , direct photon production is insensitive to symmetry potential at the studied reaction energy. For thermal photon, the curves of $V_{asy}^{(0)}$ and $V_{asy}^{(1)}$ have the nearly same multiplicities with time evolution, and they are intermediate between $V_{asy}^{(2)}(0.5)$ and $V_{asy}^{(2)}(2)$. We note that thermal photon production is sensitive to γ -parameter in symmetry potential $V_{asy}^{(2)}(\gamma)$, i.e. less γ , corresponds to softer symmetry energy, induces more ther-

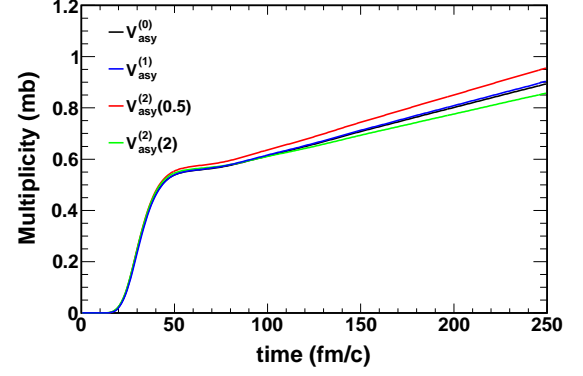


FIG. 14: (Color online) Time evolution of hard photon multiplicity with different symmetry potentials for the reaction $^{48}\text{Ca} + ^{48}\text{Ca}$ at 60A MeV.

mal photons. And we also note that the sensitivity of thermal photon production to γ is not remarkable in comparison with its sensitivity to the incompressibility K , which is of course understandable since the symmetry energy is relative small term in comparison with the incompressibility K .

From the effects of the incompressibility and symmetry potential on hard photon production, it appears that the yield of thermal photons has rather strong dependence on nuclear compressibility as well as symmetry energy, whereas the yield of direct photons is rather insensitive to nuclear EOS. Therefore thermal hard photon could serve as a probe of nuclear EOS in intermediate energy HIC.

V. PHOTON-PHOTON CORRELATIONS

In above sections, we mainly focus on the properties of inclusive hard photons, from which we find that production distribution and anisotropic flows of hard photons reveal rich information of nuclear dynamics. Also, the sensitivity to the nuclear equation of state and symmetry energy for hard photons has been discussed. In this section, we will discuss the correlation properties of photons in terms of two-particle correlation technique that can provide us a very powerful tool to characterise the properties of a particle source. In particular, two-boson relative momentum distributions enable one to determine the space-time structure according to the formalism of Bose-Einstein correlations. The magnitude of the correlation can be related to their space-time distribution of the boson source. In the following calculations, we will construct two-photon momentum correlation function as well as azimuthal correlation function, from which the space-time structure of the photon source and anisotropy property can be indicated.

A. Two-photon momentum correlation

Intensity interferometry (also called HBT correlation) is used as a universal tool to study the properties of any boson sources such as stars [45], or photon and meson sources in the early phase of heavy-ion collisions [46]. The formalism was developed starting from optics and quantum statistics and was finally adapted to the dynamics of heavy-ion collisions [47–55]. We have performed the calculation which evaluates the correlation function directly from the photon source distribution given by the BUU calculation. We store for each i th pn collision its position \vec{r}_i and the associated photon probability distribution $P_i(\vec{k}_i)$. After the completion of the calculation, we analyze this output data to construct plane waves with four-momentum \vec{k}_i at \vec{r}_i and calculate the two-photon probability for $i \neq j$ as [38, 56]:

$$P_{12} = P_1 \otimes_2 \left| A e^{i(\vec{k}_1 \cdot \vec{r}_i + \vec{k}_2 \cdot \vec{r}_j)} + B e^{i(\vec{k}_1 \cdot \vec{r}_j + \vec{k}_2 \cdot \vec{r}_i)} \right|^2 \quad (15)$$

$$= P_1 \otimes_2 [1 + 2AB \cos[q(\vec{r}_i - \vec{r}_j)]] , \quad (16)$$

where $P_1 \otimes_2$ represents the probability to produce a pair without correlation, and A and B are the amplitudes related to the normalized probabilities of the direct $[P_i(\vec{k}_1)P_j(\vec{k}_2)]$ and cross terms $[P_j(\vec{k}_1)P_i(\vec{k}_2)]$. This corresponds to Fourier transforming the photon source event by event. We set the weight of the interference in Eq. 16 as κ , that is $\kappa = 2AB$, which was predicted between 0.5 and 1.0 depending on the anisotropy of hard photon emission. The exact experimental filter was finally applied to the projection onto the Lorentz-invariant relative four momentum $Q = \sqrt{q^2 - q_0^2}$ of the resulting distribution P_{12} and $P_1 \otimes_2$ of Eq. 16, then the two-photon correlation function was calculated as $C_{12}(Q) = \frac{P_{12}}{P_1 \otimes_2} = 1 + \kappa \cos[q(\vec{r}_i - \vec{r}_j)] = f(Q)$.

For convenience, κ was set to 0.75 for our calculations in order to take into account the established anisotropic component in the angular distribution of hard photons. The two-photon correlation function has been fitted with a Gaussian parameterization with correlation strength λ and radius parameter R_Q :

$$C_{12} = 1 + \lambda \exp(-Q^2 R_Q^2). \quad (17)$$

In the above relation R_Q is the space-time parameter conjugate to Q , which measures an invariant length depending on the source-size parameters R and τ :

$$R_Q = R \sqrt{\frac{1 + (\tau/R)^2 (q_0/q)^2}{1 - (q_0/q)^2}}. \quad (18)$$

One can easily know that, since $q_0 \ll q$, R_Q is a first order measure of the spatial extent of the source, that is $R \approx R_Q$. We can then calculate from R_Q the rms radius of the source as the one of a static three-dimensional Gaussian source: $R_{rms} = \sqrt{3}R_Q$.

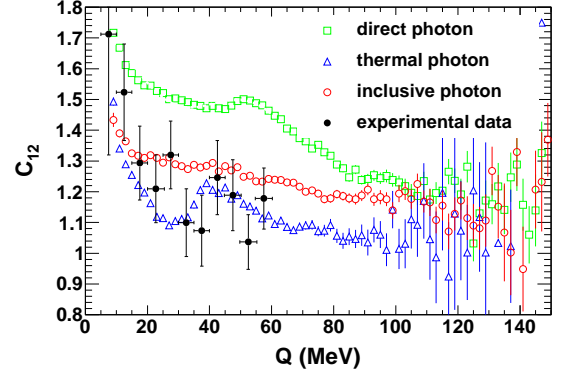


FIG. 15: (Color online) Two-photon HBT correlation function for the reaction $^{86}\text{Kr} + ^{58}\text{Ni}$ collisions at 60A MeV in the laboratory frame, $E_\gamma > 25$ MeV. The green squares represent for direct photons, blue triangles for thermal photons, and red open circles for inclusive photons. The black closed circles represent for the experimental data taken from Ref. [38, 39].

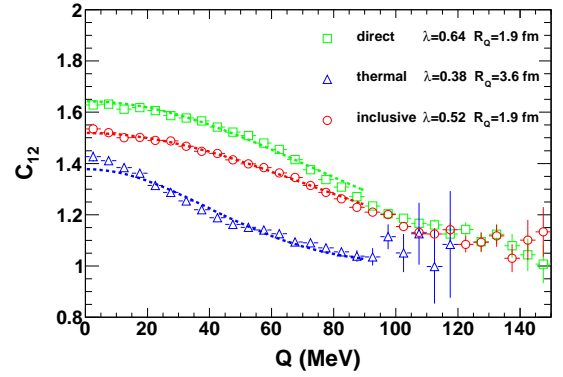


FIG. 16: (Color online) Two-photon HBT correlation function for the reaction $^{40}\text{Ca} + ^{40}\text{Ca}$ collisions at 60A MeV. The symbols are the same as Fig. 15 and the dashed lines are fitting functions as Eq. 17.

For the comparisons with experimental data, we calculated the reaction $^{86}\text{Kr} + ^{58}\text{Ni}$ at 60A MeV, employing here the following filter which is very similar to the experiment: $E_\gamma(1,2) > 25$ MeV, detector positions between polar angles of 35° and 165° (orienting downstream), azimuthal opening angles of $0 \pm 28^\circ$ and $180 \pm 28^\circ$, and 18° for the minimum opening angle. Fig. 15 presents HBT correlation functions of direct photons (green squares), thermal photons (blue triangles) and inclusive photons (red open circles), respectively. We find that the correlation function of direct photons is much larger than thermal one, and the correlation function of inclusive photons is intermediate. This result is reasonable, because direct photons are emitted at the early compressed stage of collisions, so they have stronger interference than thermal photons which are produced in later thermalizing stage. We also see that our result can well reproduce the experimental data [38, 39], especially for the correlation function of thermal photons, which agrees with

the experimental function even the oscillation structure. Therefore, we can successfully reproduce the HBT correlation function of hard photons by the BUU simulation

In order to further study the HBT correlation of hard photon and extract photon source information, we calculated the symmetric reaction system $^{40}\text{Ca} + ^{40}\text{Ca}$ at 60A MeV in the C.M. frame, and only the events of central collision ($0 < b_{red} \leq 0.2$) were taken for simplification. In Fig. 16, we find that the correlation function of direct photons is the largest, the thermal one is the least, and the correlation function of inclusive photons are between them. Moreover, in the conditions of above reaction, all of them can be well fitted by Eq. 17. After fitting correlation function, we can obtain two useful fitting parameters: correlation strength λ and radius parameter R_Q . As the results on top right corner show, direct photons have the largest correlation strength λ , the second is inclusive photons and the least one is thermal photons. Thus λ is a parameter which is sensitive to the intensity of interference. And we also get three radius parameters R_Q . R_Q of thermal photons is nearly twice than direct photons', and inclusive photon is equivalent to the later. To explain this, we know that direct photon is mostly emitted in the early stage when the reaction system is strongly compressed, so the emission source of photons is small. And later on, the thermalizing system extends very much in company with the production of thermal photons. In this reaction energy at $E_{lab} = 60A$ MeV, most of hard photons are produced in the early stage of the collision, so the spatial source extent of inclusive photons should be approximate to the direct photons. As a result, they have equivalent radius parameter R_Q . Then we can get the rms radius of the photon source by the equation $R_{rms} = \sqrt{3}R_Q$. Therefore, two-photon correlation function provides the information of hard photon source, which is available to investigate the emission source during the collisions.

B. Two-photon azimuthal correlation

From individual-photon azimuthal distribution, we find that direct hard photons exhibit the azimuthal asymmetric emission in intermediate energy heavy-ion collisions, especially negative elliptic flow parameter v_2 . Actually it is difficult to extract the elliptic flow parameter v_2 by the method of reconstructing reaction plane in the experiment, so as below, we will discuss to use the method of two-photon azimuthal correlation to extract the elliptic flow of direct photons directly.

For particles in the same class, we defined the particle azimuthal correlation function following the multi-fragment azimuthal correlation method [29, 57, 58]. The multi-fragment azimuthal correlation function is defined as follows:

$$C(\Delta\phi) = \frac{N_{cor}(\Delta\phi)}{N_{uncor}(\Delta\phi)}, \quad (19)$$

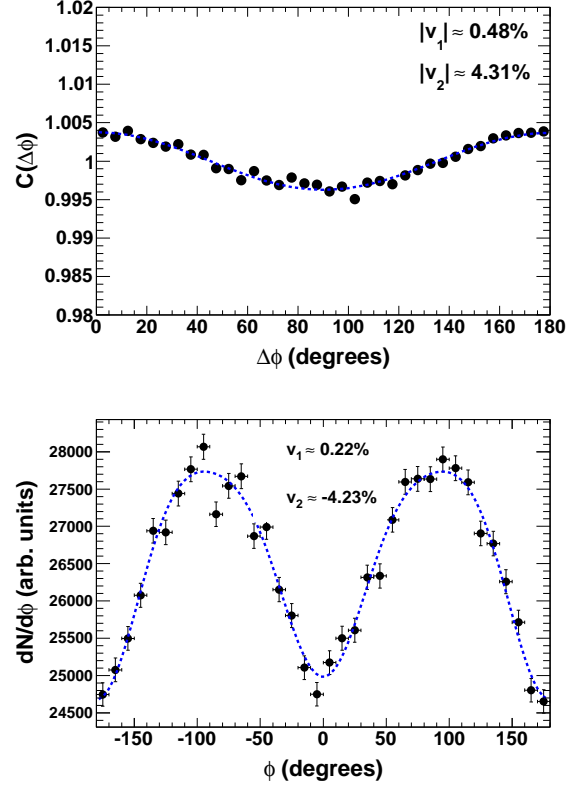


FIG. 17: (Color online) Top panel: Two-photon azimuthal correlation function for the reaction $^{40}\text{Ca} + ^{40}\text{Ca}$ at 60A MeV for semi-central events (40%–60%), and the dashed line is the fitting function as Eq. 20; Bottom panel: Individual-photon azimuthal distribution for the same reaction, and the dashed line is a fit of Fourier expansion.

where N_{cor} is the $\Delta\phi$ distribution for fragment pairs from the same event and N_{uncor} is the $\Delta\phi$ distribution by randomly selecting each member of a fragment pair to form mixed events. The $\Delta\phi$ between all selected fragments in an event are used to construct the correlation function, that is, $\frac{n(n-1)}{2}\Delta\phi$ angles for n fragments.

In our calculations for two-photon azimuthal correlations, we get N_{cor} from the $\Delta\phi$ distribution of photon pairs in the same event and N_{uncor} from the mixed events. For these correlations, we may make a fit of the Fourier series with the expression

$$C(\Delta\phi) = A[1 + \lambda_1 \cos(\Delta\phi) + \lambda_2 \cos(2\Delta\phi)], \quad (20)$$

where λ_1 and λ_2 are treated as fit parameters.

Under the assumption of statistically independent emission of particles with the same azimuthal distribution $F(\phi)$ in an event, the azimuthal correlation function is simply related to $F(\phi)$ via the convolution

$$C(\Delta\phi) = \int_0^{2\pi} F(\phi)F(\phi + \Delta\phi)d\phi. \quad (21)$$

One the other hand, $F(\phi)$ can be described by the

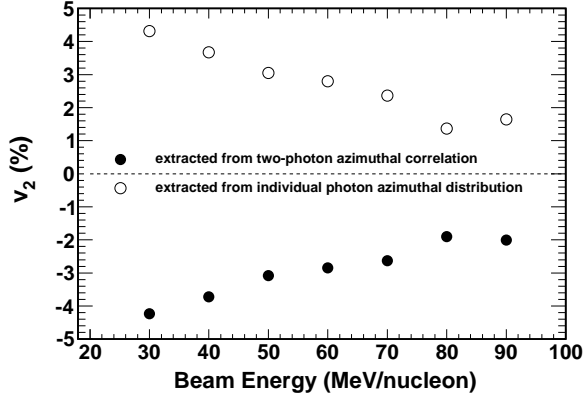


FIG. 18: Excitation function of v_2 for reaction $^{40}\text{Ca} + ^{40}\text{Ca}$ at 60A MeV with centrality 40%–60%, open circles represent the amplitude of v_2 extracted from two-photon azimuthal correlation and red ones from the fit of Fourier expansion to individual-photon azimuthal distribution.

Fourier expansion:

$$F(\phi) = \frac{dN}{d\phi} \propto 1 + 2 \sum_{n=1}^{\infty} v_n \cos(n\phi), \quad (22)$$

where the different n th harmonic Fourier expansion coefficient v_n is defined as the n th anisotropic flow, of which v_1 is directed flow parameter and v_2 is so called elliptic flow parameter.

If we only take v_1 and v_2 terms in Eq. 22 and substitute Eq. 22 into Eq. 21, we can derive the form of $C(\Delta\phi)$ as follows:

$$C(\Delta\phi) = B[1 + 2v_1^2 \cos(\Delta\phi) + 2v_2^2 \cos(2\Delta\phi)] \quad (23)$$

From Eq.21 and Eq.22, we then get the relationship between the fitted parameter λ_2 and the elliptic flow parameter v_2 [29]:

$$|v_2| \approx \sqrt{\lambda_2/2}. \quad (24)$$

Now we make the comparison of elliptic flow parameter v_2 extracted from two-photon azimuthal correlation with fitting value from individual-photon azimuthal distribution. In Fig. 17, we calculated the reaction $^{40}\text{Ca} + ^{40}\text{Ca}$ at 60A MeV for semi-central events (40%–60%) with the compressibility $K = 235$ MeV, and we extracted the elliptic flow parameters v_2 by the two distinct methods above. Then we can see that the absolute values of v_2 are nearly equivalent, except that we can only get the amplitude of elliptic flow from two-photon azimuthal correlation, and the fitting value of v_2 from individual-photon azimuthal distribution is negative. Further, as shown in Fig. 18, we get the excitation function of v_2 by the above two methods which shows nearly same amplitude of v_2 in various reaction energy but different signs. Therefore, in view

of the difficulty to reconstruct reaction plane in experiment, two-photon azimuthal correlation provides us an alternative method to extract the amplitude of elliptic flow parameter v_2 of hard photons.

VI. SUMMARY

In summary, we have systematically investigated hard photon production by the process of proton-neutron bremsstrahlung as well as the behavior of azimuthal asymmetry of hard photons and free protons produced in intermediate energy heavy-ion collisions in the framework of the BUU model. As discussed in previous studies, hard photons can be separated into direct hard photon which is produced by the first channel neutron-proton bremsstrahlung and thermal hard photon which is produced by the later stage neutron-proton bremsstrahlung during the system's evolution towards thermalization. The kinetic energy spectra of two kinds of photons show the exponential form which provides us with information on the apparent temperature in different stage of heavy-ion collision.

The azimuthal asymmetry parameters have been investigated in detail. The time evolution of directed flow and elliptic flow of hard photons exhibits rich structure as the density of the system oscillates during the pre-equilibrium and thermalization stage of reaction system. This structure indicates that the azimuthal asymmetry evolves with time. A nonzero directed transverse flow and elliptic flow parameter have been predicted for the direct hard photons produced by the first channel proton-neutron bremsstrahlung process in the intermediate energy heavy-ion collisions. The asymmetry parameters of hard photons are plotted as a function of rapidity and transverse momentum, which show contrary signs in comparison with the flow of free protons, i.e. the azimuthal asymmetry of direct hard photons seems to be anticorrelated to that of the corresponding free proton's. Therefore we can expect the direct hard photon can server as a good probe to nuclear matter properties in the early stage of HIC.

Different variables dependences are investigated for the hard photon production and anisotropic flow. We can see that the absolute value of both directed flow and elliptic flow of direct photons and free protons increase with the impact parameter, indicating that the flow mainly reflects the initial geometric asymmetry of the collision zone in a given beam energy and revealing a rich structure of flows with increasing beam energy. For directed flow, direct photons reach a minimum of around 40A MeV where the free protons approach the maximum negative value, while for elliptic flow, the absolute values of direct photons show decreasing trends with increasing beam energy. The EOS dependence for hard photons at different time indicates that the direct photon is not sensitive to the nuclear incompressibility nor to the symmetry energy. However, for the thermal photon, its mul-

tiplicity increases with nuclear incompressibility. For a given nuclear incompressibility, the soft symmetry energy favors thermal photon production.

Finally, we calculated the two-photon correlations, including HBT momentum correlations and azimuthal correlations. From two-photon HBT correlations, we can extract photon source information, such as intensity interference and the spatial extent of the emission source. We also find that two-photon azimuthal correlations can provide us with a good method for extracting the amplitude of the elliptic flow parameter v_2 of hard photons in the experiment.

In light of the present study, we expect that direct photons would be a very useful probe for exploring nuclear

reaction dynamics in intermediate energy heavy-ion collisions, while the thermal hard photon can give us some hints on the nuclear EOS, including the symmetry energy.

Acknowledgements

This work is supported partially by the Knowledge Innovation Project of Chinese Academy of Sciences under Grant No. KJCX2-EW-N01, the National Natural Science Foundation of China under contract No.s 11005140, 11035009, 10979074, 10875160, 10805067 and 10975174.

-
- [1] Y. Schutz, G. Martínez, F.M. Marqués, A. Marín, T. Matulewicz, R.W. Ostendorf, P. Bożek, H. Delagrange, J. Díaz, M. Franke, K.K. Gudima, S. Hlaváč, R. Holzmann, P. Lautridou, F. Lefèvre, H. Löhner, W. Mittig, M. Ploszajczak, J.H.G. van Pol, J. Québert, P. Roussel-Chomaz, A. Schubert, R.H. Siemssen, R.S. Simon, Z. Sulkowski, V.D. Toneev, V. Wagner, H.W. Wilschut, Gy. Wolf, Nucl. Phys. A **622**, 404 (1997).
 - [2] W. Cassing, V. Metag, U. Mosel, K. Niita, Phys. Rep. **188**, 363 (1990).
 - [3] A. Bonasera, R. Coniglione, and P. Sapienza, Euro. Phys. J. A **30**, 47 (2006).
 - [4] H. Nifenecker and J. A. Pinston, Annu. Rev. Nucl. Part. Sci. **40**, 113 (1990).
 - [5] R. Wada, D. Fabris, K. Hagel, G. Nebbia, Y. Lou, M. Gonnin, J. B. Natowitz, R. Billerey, B. Cheynis, A. Demeyer, D. Drain, D. Guinet, C. Pastor, L. Vagneron, K. Zaid, J. Alarja, A. Giorni, D. Heuer, C. Morand, B. Viano, C. Mazur, C. Ng, S. Leray, R. Lucas, M. Ribrag, and E. Tomasi Phys. Rev. C **39**, 497 (1989).
 - [6] Y. Schutz *et al.* (TAPS Collaboration), Nucl. Phys. A **599**, 97 (1996).
 - [7] Y. Schutz *et al.* (TAPS Collaboration), Nucl. Phys. A **630**, 126 (1998).
 - [8] G. Martinez, F.M. Marqués, Y. Schutz, Gy. Wolf, J. Díaz, M. Franke, S. Hlaváč, R. Holzmann, P. Lautridou, F. Lefèvre, H. Löhner, A. Marín, T. Matulewicz, W. Mittig, R.W. Ostendorf, J.H.G. van Pol, J. Québert, P. Roussel-Chomaz, A. Schubert, R.H. Siemssen, R.S. Simon, Z. Sulkowski, V. Wagner, H.W. Wilschut, Phys. Lett. B **349**, 23 (1995).
 - [9] D. G. d'Enterria, L. Aphecetche, A. Chbihi, H. Delagrange, J. Díaz, M. J. van Goethem, M. Hoefman, A. Kugler, H. Löhner, G. Martínez, M. J. Mora, R. Ortega, R. W. Ostendorf, S. Schandman, Y. Schutz, R. H. Siemssen, D. Stracener, P. Tlustý, R. Turrisi, M. Volkerts, V. Wagner, H. W. Wilschut, and N. Yahli, Phys. Rev. Lett. **87**, 022701 (2001).
 - [10] A. Adare *et al.* (PHENIX Collaboration), Phys. Rev. Lett. **104**, 132301 (2010).
 - [11] J. L. Long, Z. J. He, Y. G. Ma, B. Liu, Phys. Rev. C **72**, 064907 (2005); Nucl. Phys. A **766**, 201 (2006).
 - [12] F. M. Liu, T. Hirano, K. Werner, and Y. Zhu, Phys. Rev. C **79**, 014905 (2009).
 - [13] M. M. Aggarwal *et al.* (WA98 Collaboration), Phys. Rev. Lett. **85**, 3595 (2000).
 - [14] W. Bauer, G. F. Bertsch, W. Cassing, U. Mosel, Phys. Rev. C **34**, 2127 (1986).
 - [15] G. F. Bertsch, S. Das Gupta, Phys. Rep. **160**, 189 (1988).
 - [16] J. D. Jackson, Classical Electrodynamics (Wiley, New York, 1962), p. 733.
 - [17] W. Cassing, T. Biro, U. Mosel, M. Tohyama, W. Bauer, Phys. Lett. B **181**, 217 (1986).
 - [18] G. H. Liu, Y. G. Ma, X.Z. Cai, D.Q. Fang, W.Q. Shen, W.D. Tian, K. Wang, Phys. Lett. B **663**, 312 (2008).
 - [19] F. M. Marqués, G. Martínez, Y. Schutz, J. Díaz, M. Franke, S. Hlaváč, R. Holzmann, P. Lautridou, F. Lefèvre, H. Löhner, A. Marín, T. Matulewicz, W. Mittig, R.W. Ostendorf, J.H.G. van Pol, J. Québert, P. Roussel-Chomaz, A. Schubert, R.H. Siemssen, R.S. Simon, Z. Sulkowski, V. Wagner, H.W. Wilschut, Gy. Wolf, Phys. Lett. B **349**, 30 (1995).
 - [20] A. Corsi, O. Wieland, V.L. Kravchuk, A. Bracco, F. Camera, , G. Benzoni, N. Blasi, S. Brambilla, F.C.L. Crespi, A. Giussani, S. Leoni, B. Million, D. Montanari, A. Moroni, F. Gramegna, A. Lanchais, P. Mastinu, M. Brekiesz, M. Kmiecik, A. Maj, M. Bruno, M. D'Agostino, E. Geraci, j. G. Vannini, S. Barlini, G. Casini, M. Chiari, A. Nannini, A. Ordine, M. Di Toro, C. Rizzo, M. Colonna, V. Barank, Phys. Lett. B **679**, 197 (2009).
 - [21] V. Baran, C. Rizzo, M. Colonna, M. DiToro, D. Pierrousakou, Phys. Rev. C **79**, 021603(R) (2009).
 - [22] H. L. Wu, W. D. Tian, Y. G. Ma, X. Z. Cai, J. G. Chen, D. Q. Fang, W. Guo, and H. W. Wang, Phys. Rev. C **81**, 047602 (2010).
 - [23] A. Bonasera, F. Gulminelli, J. Molitoris, Phys. Rep. **243**, 1 (1994).
 - [24] J. Y. Ollitrault, Phys. Rev. D **46**, 229 (1992).
 - [25] S. Voloshin, Y. Zhang, Z. Phys. C **70**, 665 (1996).
 - [26] H. Sorge, Phys. Lett. B **402**, 251 (1997); Phys. Rev. Lett. **78** (1997) 2309; **82**, 2048 (1999).
 - [27] P. Danielewicz, R. A. Lacey, P. B. Gossiaux, C. Pinkenburg, P. Chung, J. M. Alexander, and R. L. McGrath, Phys. Rev. Lett. **81**, 2438 (1998).
 - [28] Y. G. Ma, W. Q. Shen, J. Feng, Y. Q. Ma, Phys. Rev. C **48**, R1492 (1993); Z. Phys. A **344**, 469 (1993); Y. G. Ma, W. Q. Shen, Z. Y. Zhu, Phys. Rev. C **51**, 1029 (1995); Y.G. Ma, T.Z. Yan, X.Z. Cai, J.G. Chen, D.Q. Fang, W.

- Guo, G.H. Liu, C.W. Ma, E.J. Ma, W.Q. Shen, Y. Shi, Q.M. Su, W.D. Tian, H.W. Wang, K. Wang, Nucl Phys. A **787**, 611c (2007).
- [29] Y. G. Ma and W. Q. Shen, Phys. Rev. C **51**, 3256 (1995).
- [30] Y. M. Zheng, C. M. Ko, B. A. Li, and B. Zhang, Phys. Rev. Lett. **83**, 2534 (1999).
- [31] D. Persram and C. Gale, Phys. Rev. C **65**, 064611 (2002).
- [32] J. Lukasik *et al.* (INDRA-ALDAIN Collaboration), Phys. Lett. B **608**, 223 (2004).
- [33] T. Z. Yan, Y. G. Ma, X. Z. Cai, J. G. Chen, D. Q. Fang, W. Guo, C. W. Ma, E. J. Ma, W. Q. Shen, W. D. Tian, K. Wang, Phys. Lett. B **638**, 50 (2006).
- [34] J. H. Chen, Y. G. Ma, G. L. Ma, X. Z. Cai, Z. J. He, H. Z. Huang, J. L. Long, W. Q. Shen, C. Zhong, and J. X. Zuo, Phys. Rev. C **74**, 064902 (2006).
- [35] M. M. Aggarwal *et al.* (WA98 Collaboration), Phys. Rev. Lett. **93**, 022301 (2004); Nucl. Phys. A **762**, 129 (2005).
- [36] S. S. Adler *et al.* (PHENIX Collaboration), Phys. Rev. Lett. **96**, 032302 (2006).
- [37] S. Turbide, C. Gale, R. J. Fries, Phys. Rev. Lett. **96**, 032303 (2006).
- [38] H. W. Barz, B. Kampfer, G. Wolf, W. Bauer, Phys. Rev. C **53**, R553 (1996).
- [39] F. M. Marques, G. Martinez, T. Matulewicz, R. W. Ostendorf, Y. Schutz, Phys. Rev. C **54**, 2783 (1996).
- [40] V. Herrmann, J. Speth, K. Nakayama, Phys. Rev. C **43**, 394 (1991).
- [41] Y. Safkan, T. Akdogan, W. A. Franklin, J. L. Matthews, W. M. Schmitt, V. V. Zelevinsky, P. A. M. Gram, T. N. Taddeucci, S. A. Wender, S. F. Pate, Phys. Rev. C **75**, 031001 (2007).
- [42] H. Heiselberg and M. Hjorth-Jensen, Phys. Rep. **328**, 237 (2000).
- [43] B. A. Li, A. T. Sustich, and B. Zhang, Phys. Rev. C **64**, 054604 (2001).
- [44] A. M. Lane, Nucl. Phys. A **35**, 676 (1962).
- [45] R. Hanbury-Brown and R.Q. Twiss, Philos. Mag. **45**, 663 (1954).
- [46] G. Goldhaber, S. Goldhaber, W. Lee, A. Pais, Phys. Rev. **120**, 300 (1960).
- [47] B. Lörstad, Int. J. Mod. Phys. A **4**, 2861 (1989).
- [48] D.H. Boal, C. K. Gelbke, B. K. Jennings, Rev. Mod. Phys. **62**, 553 (1990).
- [49] J. Québert, Ann. Phys. Fr. **17**, 99 (1992).
- [50] S. E. Koonin, Phys. Lett. B **70**, 43 (1977).
- [51] S. Pratt, Phys. Rev. Lett. **53**, 1219 (1984).
- [52] W. G. Lynch, C. B. Chitwood, M. B. Tsang, D. J. Fields, D. R. Klesch, C. K. Gelbke, G. R. Young, T. C. Awes, R. L. Ferguson, F. E. Obenshain, F. Plasil, R. L. Robinson, A. D. Panagiotou, Phys. Rev. Lett. **51**, 1850 (1983).
- [53] F. M. Marques, G. Martinez, T. Matulewicz, R. W. Ostendorf, Y. Schutz, Phys. Rep. **284**, 91 (1997).
- [54] Y. B. Wei, Y. G. Ma, W. Q. Shen, G. L. Ma, K. Wang, X. Z. Cai, C. Zhong, W. Guo, J. G. Chen, Phys. Lett. B **586**, 225 (2004).
- [55] Y. G. Ma, Y. B. Wei, W. Q. Shen, X. Z. Cai, J. G. Chen, J. H. Chen, D. Q. Fang, W. Guo, C. W. Ma, G. L. Ma, Q. M. Su, W. D. Tian, K. Wang, T. Z. Yan, C. Zhong, and J. X. Zuo, Phys. Rev. C **73**, 014604 (2006); Y. G. Ma, X. Z. Cai, J. G. Chen, D. Q. Fang, W. Guo, G. H. Liu, C. W. Ma, E. J. Ma, W. Q. Shen, Y. Shi, Q. M. Su, W. D. Tian, H. W. Wang, K. Wang, Y. B. Wei, T. Z. Yan, Nucl. Phys. A **790**, 299c (2007).
- [56] M. Marqués, R. W. Ostendorf, P. Lautridou, F. Lefevre, T. Matulewicz, W. Mittag, P. Roussel-Chomaz, Y. Schutz, J. Québert, J. Díaz, A. Marín, G. Martínez, R. Holzmann, S. Hláváč, A. Schubert, R. S. Simon, V. Wagner, H. Löhner, J. H. G. van Pol, R. H. Siemssen, H. W. Wilschut, M. Franke, Z. Sujkowski, Phys. Rev. Lett. **73**, 34 (1994); F. M. Marqués, G. Martinez, T. Matulewicz, R. W. Ostendorf, Y. Schutz, Phys. Rev. C **54**, 2783 (1996).
- [57] S. Wang, Y. Z. Jiang, Y. M. Liu, D. Keane, D. Beavis, S. Y. Chu, S. Y. Fung, and M. Vient, C. Hartnack, H. Stöcker, Phys. Rev. C **44**, 1091 (1991).
- [58] R. A. Lacey, A. Elmaani, J. Lauret, T. Li, W. Bauer, D. Craig, M. Cronqvist, E. Gualtieri, S. Hannuschke, T. Reposeur, A. Vander Molen, G. D. Westfall, W. K. Wilson, J. S. Winfield, J. Yee, S. Yennello, A. Nadasen, R. S. Tickle, and E. Norbeck, Phys. Rev. Lett. **70**, 1224 (1993).